Carbon Nitride Mediated Synthesis of Titanium-Based Electrodes for High-Performance Asymmetric Supercapacitors

Wenwen Liu,[1, ¶] Jian Liang Cheong,[1, ¶] Man-Fai Ng,[2] and Jackie Y. Ying[1, 3*]

[1] NanoBio Lab, Institute of Materials Research and Engineering (IMRE), Agency for Science, Technology and Research (A*STAR), 31 Biopolis Way, Nanos #09-01, Singapore 138669, Republic of Singapore

[2] Institute of High Performance Computing (IHPC), Agency for Science, Technology and Research (A*STAR), 1 Fusionopolis Way, Connexis #16-16, Singapore 138632, Republic of Singapore

[3] NanoBio Lab, A*STAR Infectious Diseases Labs (ID Labs), A*STAR, 31 Biopolis Way, Nanos #09-01, Singapore 138669, Republic of Singapore

[¶] These authors contribute equally to this work.

[*] *Co-corresponding author*. E-mail address: jyying@imre.a-star.edu.sg

Abstract

Rational design of electrode materials with specific compositions and unique morphological and structural features to achieve supercapacitors (SCs) with high energy densities without compromising their inherent electrochemical merits remains a great challenge. Herein, a carbon nitride (C_3N_4) mediated "one-for-two" strategy was proposed to synthesize titanium nitride/carbon nanosheets (TiN/C) and titanium carbide/carbon nanosheets (TiC/C) with three-dimensional morphology and hierarchical structure, respectively. The derived TiN/C and TiC/C were used as

cathode and anode materials, respectively, with excellent capacitor behavior in aqueous electrolyte. Specifically, asymmetric SCs constructed with the TiN/C cathode and the TiC/C anode delivered a large operation voltage of 0.3–1.8 V, a high specific capacitance of 103 $F \cdot g^{-1}$, and a remarkable energy density of 45.2 $Wh \cdot kg^{-1}$, outperforming most of the previously reported TiN- and TiC-based SCs. *Ex situ* XRD and TEM characterizations as well as DFT simulation indicated that the excellent performance could be attributed to reversible pseudocapacitive redox reaction and electro-adsorbed anions at the TiN/C cathode, and fast adsorption/desorption of cations at the TiC/C anode, as well as unique surface morphology and heterostructure. The strategy presented in this work also provides new design concepts for the synthesis of other transition metal nitrides (or carbides)/carbon composites for other advanced energy applications.

Keywords

Asymmetric supercapacitors; “one-for-two” strategy; advanced electrode; titanium nitride/carbon nanosheets; titanium carbide/carbon nanosheets

1. Introduction

The limited fossil fuel reserve, the growing environmental problems, as well as the increased use of electric vehicles and wearable/portable electric devices have led to great interest in developing energy storage and conversion systems.[1, 2] Supercapacitors (SCs) are attractive due to their larger specific capacitance than the traditional capacitors, higher rate ability and better cycling durability than conventional batteries.[1] Despite these advantages, SCs often suffer from relatively low energy density, which limits their broad and practical applications.[3, 4] Increasing specific capacitance and/or enlarging operating voltage are the straightforward approaches towards achieving SCs with the desired energy density. In this respect, new design and rational construction

of asymmetric SCs with advanced cathode and anode materials could be highly effective in boosting the energy density in two aspects: (1) extending the voltage through asymmetric SC configuration, and (2) enhancing specific capacitance of both cathode and anode via advanced functional nanomaterials.

To date, substantial research efforts have been devoted towards developing pseudocapacitive materials due to their attractive intrinsic physicochemical properties, such as high theoretical capacitance and chemical stability. However, majority of these traditional pseudocapacitive materials (e.g., metal oxides, metal hydroxides and conducting polymers) usually encounter some drawbacks, such as relatively poor rate capability caused by their low conductivity and poor cycling stability, which hinder their practical implementations.[5, 6] On the other hand, transition metal nitrides and carbides (e.g., VN, Nb_4N_5, MoN, Mo_2C, NbC, V_2C and WC) represent an emerging class of pseudocapacitive materials.[7-11] In particular, titanium nitride (TiN) and carbide (TiC) are very attractive due to their unique properties, such as large theoretical capacitance, high electronic conductivity, and excellent thermal stability.[10-14] However, the short cycle lifetime and mediocre specific capacitance have impeded their applications.[15-17] Strategies to overcome these drawbacks have been developed with varying degrees of success, but the electrochemical performance remains unsatisfactory.[18, 19] Hence, it would be of great interest to develop better TiN and TiC electrode materials to address the aforementioned issues, and achieve SCs with excellent performance.

Besides the intrinsic properties of the electrode materials, the supercapacitive performance is dependent on the morphology, surface chemistry and porosity of the materials.[20] These physicochemical characteristics have significant impact on the active sites, ion transport, electron transfer, and active material utilization, which are strongly associated with the electrochemical

performance (e.g., capacitance, rate capability and cycle stability) of the pseudocapacitive materials.[2, 5, 6] Development of electrode materials with unique morphological and structural features can significantly boost their capacitor behavior. Moreover, incorporation of advanced carbon materials (especially heteroatom-doped carbon materials) into the pseudocapacitive materials can endow the electrode materials with enhanced ion/electron conductivity and wettability, larger electrolyte contact area, and better mechanical stability, [1, 9, 16, 21] thereby improving their electrochemical performance.

Based on the above considerations, a carbon nitride (C_3N_4) mediated "one-for-two" strategy has been developed to synthesize TiN/C nanosheets and TiC/C nanosheets as electrode materials with unique three-dimensional (3D) morphology and hierarchical nanostructure. Compared to the previously reported cathode and anode materials prepared by the traditional method starting from two different precursors,[22] our two electrodes derived from the same precursor would not only share similar morphological and structural characteristics, but also provide synergistic effects to enhance their respective physicochemical properties, bringing about unique characteristics and excellent electrochemical performance. The TiN/C cathode and TiC/C anode materials led to an asymmetric SC with a large potential window of 0.3–1.8 V, a high specific capacitance of 103 $F \cdot g^{-1}$, and an energy density of 45.2 $Wh \cdot kg^{-1}$, which were superior to most reported TiN- and TiC-based SCs. This "one-for-two" design strategy can also be extended to the design and synthesis of other transition metal nitride and carbide materials for a diverse range of energy storage and conversion applications.

2. Results and discussion

2.1. Titanium Nitride/Carbon Nanosheet (TiN/C) Cathode

The preparation of TiN/C nanocomposite is illustrated in Figure 1a. Briefly, C_3N_4 nanosheets were first synthesized by calcination of urea in air, followed by ultrasonic exfoliation (Figures S1a and S2). Titanium butoxide was then added to the C_3N_4/tetrahydrofuran (THF) dispersion under rigorous stirring. THF solvent was subsequently removed by evaporation, and the resulting mixture was heat-treated in an inert argon atmosphere. TiN/C nanocomposite was obtained upon cooling the sample to room temperature (Figure S1b). By controlling the calcination temperature, TiC/C nanocomposite could also be achieved using a similar process (Figure S1c). In this "one-for-two" strategy, C_3N_4 functioned as a mediating agent, which not only served as the gas source of nitridation by self-decomposition to facilitate the synthesis of TiN/C, but also acted as the carbon source for preparing TiC/C through carbothermal reaction. As shown in Figure 1b, TiN/C nanocomposite has a nanosheet-like morphology with typical folding and wrinkling features, forming a unique interconnected 3D structure that could facilitate electrolyte ion access and shorten ion diffusion distance. Low-resolution transmission electron microscopy (TEM) images (Figures 1c and d) reveal that the ultrafine TiN nanoparticles were anchored on carbon nanosheets, which would provide better contacts, more charge storage active sites, and faster electron transfer pathways. This unique structure also would help to maintain the structure integrity of TiN during cycling. High-resolution TEM (HR-TEM) images (Figures 1e and f) show lattice fringes with a lattice spacing of 0.243 nm (Figure 1g), which was assigned to the (111) crystalline plane of TiN. Energy dispersive X-ray (EDX) spectroscopy illustrates the uniform distribution of each element in the TiN/C nanocomposite (Figure 1h).

Powder X-ray diffraction (XRD) pattern of TiN/C nanocomposite (Figure 2a) showed peaks at 36.6°, 42.7°, 61.8°, 74.2° and 78.3°, which corresponded to the cubic TiN phase (JCPDS 38-1420).[10, 11] The broad diffraction peak at 23.6° could be assigned to the (002) plane of carbon

nanosheets derived from C_3N_4.[23] A small peak was noted at 69.2°, which could be attributed to a trace amount of TiO_2 in the TiN/C nanocomposite arising from surface passivation of TiN.[24] The average crystallite size of TiN calculated with Scherrer's equation was ~ 3.2 nm for the (200) peak, which agreed well with the TEM results. Raman spectrum of TiN/C nanocomposite (Figure 2b) showed three peaks at 257, 426 and 602 cm^{-1}, which could be attributed to TiN, reflecting the presence of Ti and N ion vacancies in TiN. [25] The other two Raman peaks at 1354 and 1583 cm^{-1} were associated with the D and G bands of carbon nanosheets. The intensity ratio (I_D/I_G = 1.02) indicated the existence of rich defects in the carbon nanosheets.[26] X-ray photoelectron spectroscopy (XPS) of TiN/C nanocomposite showed peaks associated only with Ti, N, C and O elements in the survey spectrum (Figure 2c). The Ti2p core-level spectrum could be deconvoluted into six peaks (Figure 2d) at 455.8 and 461.5 eV (assigned to Ti-N), 457.1 and 463.2 eV (assigned to O-Ti-N), and 458.1 and 464.6 eV (assigned to Ti-O).[24, 27-29] The presence of Ti-O could be associated with the trace amount of TiO_2 or TiO_xN_y on TiN surface due to surface passivation.[10, 11] The N1s core-level spectrum was deconvoluted into five peaks at 396.2, 397.6, 398.7, 400.3, and 401.4 eV (Figure 2e), which could be assigned to Ti-N, O-Ti-N, pyridinic-N, pyrrolic-N, and graphitic-N, respectively. These vacancies/defects in TiN combined with heteroatom doping in carbon nanosheets could enhance the electrochemical performance of TiN/C nanocomposite by improving the wettability and providing more anchoring sites for electrolyte.[30, 31] TiN/C nanocomposite has a type-IV nitrogen adsorption-desorption isotherm (Figure 2f). It has a high Brunauer-Emmett-Teller (BET) specific surface area of 429.5 $m^2 \cdot g^{-1}$, a large pore volume of 1.43 $cm^2 \cdot g^{-1}$, and an average pore size of 10.9 nm (inset of Figure 2f). These would not only offer more active sites and promote more electrolyte ion adsorption, but also provide a more effective pathway

for electrolyte access and transport, thereby improving the electrochemical performance of TiN/C. [32]

Electrochemical behavior of the TiN/C composite was evaluated by cyclic voltammetry (CV) and galvanostatic charge/discharge (GCD) techniques. The CV curves remained quasi-rectangular in shape with gradually increasing scan rates (Figure 2g), indicating an ideal capacitive behavior and a good rate capability for the TiN/C nanocomposite. The GCD curves exhibited symmetrical triangle shapes and showed a linear relationship between potential and time (Figure 2h). There was no obvious "IR drop" in the initial section of the GCD curve, indicating that the internal resistance of the TiN/C electrode was small. The capacitance of the TiN/C nanocomposite calculated from the discharge curve was as high as 287 $F \cdot g^{-1}$ at 1 $A \cdot g^{-1}$, which was much higher than for commercial TiN (Figure S3) as well as outperforming those reported previously results (e.g., mesoporous TiN spheres,[33] TiN/C fiber,[34] TiN/VN core-shell composite,[35] core-shell TiN/VN fiber,[36] chrysanthemum-like TiN,[10, 11] MnO_2/TiN composite,[37] and TiN/graphene nanosheets [19]). The specific capacitance of the TiN/C electrode decreased with increasing current density (Figure 2i), which was attributed to the insufficient time for the diffusion and access of electrolyte. [38, 39] However, TiN/C nanocomposite retained ~ 60% of its specific capacitance when the current density was increased from 1 $A \cdot g^{-1}$ to 10 $A \cdot g^{-1}$, illustrating its good rate performance. Electrochemical impedance spectroscopy (EIS) was used to evaluate the interface dynamic behavior of the TiN/C electrode. The Nyquist plot consisted of a small quasi-semi-circle and a straight line (Figure S4). The first intercept of the quasi-semi-circle with the real axis was 1.3 Ω, and the diameter of the quasi-semi-circle was 3.6 Ω, indicating relatively small equivalent series resistance and charge transfer resistance, respectively. The slope of the straight line in

Nyquist plot was almost perpendicular to the real axis, reflecting the fast ion diffusion and superior capacitive behavior of the TiN/C nanocomposite cathode.

To better understand the electrochemical performance of the TiN/C nanocomposite electrode, density functional theory (DFT) calculations were performed to elucidate the electronic structure, interfacial charge transfer, and ion diffusion barrier of the nanomaterial (Figure 3). TiN/C nanocomposite was modelled as the heterostructure of TiN and N-doped carbon nanosheet, as shown in the inset of Figure 3b. Here, the TiN (001) lattice plane was chosen for calculations because it was the most stable and easily exposed surface based on the reported literature. [10-14] Compared with the density of states (DOS) of the pure TiN structure (Figure 3a), the TiN/C heterostructure (Figure 3b) has a larger electronic DOS in the valence band near the Fermi level (0 eV). This indicates that the electrical conductivity of the TiN/C nanocomposite was enhanced due to the orbital re-hybridization induced by the coupling between TiN and N-doped carbon nanosheet. Notably, the interfacial charge density revealed that there were strong interfacial interactions between TiN and N-doped carbon nanosheet as well as substantial charge transfer from TiN to the nanosheet (Figure 3c), which provided low interfacial resistance for electron transport, enhanced charge transfer capability, and favored the improvement of electrochemical properties.[5, 6, 12-14] Furthermore, considering that the electrode capacitance, also known as quantum capacitance, was proportional to the DOS, the larger DOS at the Fermi level corresponded to larger electrode capacitance for the TiN/C nanocomposite. In addition, to evaluate the mobility of electrolyte ions on these nanomaterials, the ion diffusion barriers were calculated (Figures 3d–f). It was found that the diffusion barrier of SO_4^{2-} was 0.79 eV on pure TiN. In contrast, it was 0.04 eV on the TiN/C nanocomposite (Figure 3f). This verified better ion transport on the TiN/C nanocomposite, thus ensuring its good rate capability and high-power density. The DFT

results showed that the TiN/C nanocomposite was a promising cathode candidate for supercapacitor due to its large quantum capacitance, enhanced electrical conductivity, and small ion diffusion barrier, which were in good agreement with our experimental results and conclusion.

2.2. Titanium Carbide/Carbon Nanosheets (TiC/C) Anode

The as-prepared TiC/C nanocomposite showed a 3D interconnected structure (Figure 4a) that consisted of nanosheets with highly wrinkled surface (Figure 4b). Its microstructure and morphology were similar to that of the TiN/C nanocomposite due to the proposed "one-for-two" strategy. The TiC nanoparticles were uniformly decorated on the carbon nanosheets (Figures 4c and d), which provided more TiC interfaces, offered more electrolytes contact area and exposed more electrochemically active sites. HR-TEM image (Figure 4e) showed lattice fringes with interplanar spacing of ~ 0.211 nm (Figure 4f), which was attributed to the (002) lattice plane of TiC. EDX elemental mapping (Figure 4g) confirmed the uniform distribution of each element in the TiC/C nanocomposite.

XRD diffraction peaks located at 36.5°, 42.5°, 61.6°, 74.0°, and 78.1° in Figure 5a were indexed to cubic TiC phase.[21] The broad peak at 23.9° could be attributed to the (002) plane of the carbon nanosheets derived from C_3N_4. These results confirmed that TiC/C nanocomposite was successfully prepared from C_3N_4, which acted as the carbon source for the carbothermal reaction as well as the precursor of the carbon nanosheets. Figure 5b shows that TiC/C has three Raman peaks in the range of 260 to 610 cm^{-1}, which corresponded to TiC. [40] The other two strong Raman peaks at 1358 and 1588 cm^{-1} were D and G bands related to the sp^3 carbon with defects and the sp^2 graphitic carbon, respectively.[41, 42] The I_D/I_G ratio of 0.93 indicated that the presence of rich defects within the carbon nanosheets. The XPS survey spectrum of TiC/C nanocomposite showed only peaks associated with Ti, C, N and O elements (Figure 5c). XPS Ti2p core-level

spectrum was fitted with six peaks (Figure 5d), which were ascribed to Ti-C bonds (454.6 and 460.3 eV), O-Ti-C bonds (455.6 and 461.5 eV) and Ti-O bonds (457.8 and 463.7 eV).[43] The C1s XPS spectrum was deconvoluted into five peaks at 282.2, 284.6, 285.6, 288.2, and 291.1 eV (Figure 5e), which could be assigned to C-Ti, C-C, C-N or C-O, C=O, and π-π*,[43, 44] respectively. The oxygen-related bonds and defects in the TiC/C nanocomposite could improve the wettability and provide additional pseudocapacitive contribution through Faradaic redox reactions. The TiC/C nanocomposite has a very high BET surface area (404.7 $m^2 \cdot g^{-1}$) and a broad pore size distribution (Figure 5f). The macropores within this hierarchical porous structure could serve as electrolyte reservoir and facilitate access of electrolyte, while the mesopores could provide more electrolytes contact area, acting as pathways for ions and shortening ion diffusion distance.

TiC/C nanocomposite electrode showed good capacitive behavior as indicated by the near-rectangular CV curves (Figure 5g) and the symmetrical triangle GCD curves (Figure 5h). From the discharge curve, the TiC/C composite achieved a specific capacitance as high as 460 $F \cdot g^{-1}$ at 1 $A \cdot g^{-1}$, 82% of this specific capacitance was retained even at 10 $A \cdot g^{-1}$ (Figure 5i), implying its superior rate performance. The specific capacitance of our TiC/C nanocomposite was much better than or comparable to the commercial TiC (Figure S5) and other reported TiC-based electrodes, such as TiC/C composite,[45] TiC/C hybrid nanofiber,[46] TiC hollow fiber-nanotube electrode,[18] and TiC hollow sphere,[47] indicating its potential as a promising electrode material for SCs. The Nyquist plot of TiC/C nanocomposite was composed of a small quasi-semicircle and an almost vertical line (Figure S6), demonstrating low equivalent series resistance (1.2 Ω), small charge transfer resistance (2.7 Ω) and fast ion diffusion.

To further understand the superior supercapacitive performance of the TiC/C nanocomposite electrode, DFT calculations were performed to investigate the electronic structure, interfacial

charge transfer, and ion diffusion barrier in this composite (Figure 6). Herein, the most stable TiC (001) lattice plane was used. It was found that the TiC/C heterostructure (Figure 6b) has a relatively larger electronic DOS in the valence band near the Fermi level as compared to that of pure TiC (Figure 6a). This indicated that the coupling between TiC and N-doped carbon nanosheet benefited the formation of hybridization orbital and resulted in charge redistribution (Figure 6c), which could accelerate the electron transport, improve the electrical conductivity, and boost the electrode capacitance. In addition, the calculated diffusion barrier of Na^+ on TiC/C nanocomposite (0.03 eV) (Figures 6d and f) was smaller than that on pure TiC (0.09 eV) (Figures 6e and f). This indicated smaller charge transport resistance in the TiC/C nanocomposite, thereby ensuring its better electrochemical performance in terms of power density and rate capability. The DFT results showed that the TiC/C nanocomposite was a promising anode candidate for supercapacitor, which was consistent with our electrochemical results.

2.3. Characterization of TiC/C//TiN/C Asymmetric Supercapacitors

A standard coin-cell type asymmetric SCs was assembled with TiN/C as cathode and TiC/C as anode to evaluate the practical application of these nanocomposites. The independent CV curves in half-cell (Figure 7a) showed that the maximum operating voltage of the TiC/C//TiN/C asymmetric SCs should be from 0.3 to 1.8 V. As the charge balance required for the cathode and anode of asymmetric SC device, the mass ratio of TiN/C cathode and TiC/C anode to maximize energy density was 1.4. The CV profiles were almost rectangular in shape (Figure 7b), demonstrating the typical capacitor behavior of the device, as well as its fast ion transport and electron transfer. The nearly symmetrical triangular GCD curves (Figure 7c) and the absence of obvious “IR drop” further indicated the typical capacitor behavior of the device and its small internal resistance. The capacitance of the cell calculated from the discharge curve was 103 $F \cdot g^{-1}$

at 0.5 $A \cdot g^{-1}$ (Figure 7d). Even with an increase of 20× in the current density (to 10 $A \cdot g^{-1}$), ~ 70% capacitance was successfully retained (73 $F \cdot g^{-1}$).

The device kept 83% of its initial capacitance after 4000 cycles (Figure 7e), indicating excellent cycling stability of the asymmetric SC. As shown in EIS plot (Figure 7f), the equivalent series resistance (R_s) underwent almost no change, while electrochemical charge transfer resistance (R_{ct}) slightly increased after cycling, which probably resulted from the loosening of active materials during cycling. To confirm this, the TiN/C cathode and the TiC/C anode were investigated by TEM and EDX mapping after cycling. Figures S7 and S8 showed that there was no obvious morphological change, and the TiN and TiC nanoparticles remained strongly anchored onto the carbon nanosheets after cycling the respective nanocomposites. Also, the crystal structure and the uniform elemental distribution were retained for the nanocomposites. Ragone plot (Figure 7g) showed that the device delivered a maximum energy density of 45.2 $Wh \cdot kg^{-1}$ at 535.3 $W \cdot kg^{-1}$ and demonstrated a high energy density of 31.9 $Wh \cdot kg^{-1}$ even at a power density as high as 9570 $W \cdot kg^{-1}$. These results were comparable or superior to other metal nitride/carbide-based asymmetric SCs or symmetric SCs, such as TiN/C//MnO_2 (17.2 $Wh \cdot kg^{-1}$ at 70 $W \cdot kg^{-1}$),[48] TiN//TiN (5 $Wh \cdot kg^{-1}$ at 1800 $W \cdot kg^{-1}$),[49] TiN/Fe_2O_3//TiN/MnO_2 (71.2 $Wh \cdot kg^{-1}$ at 499.8 $W \cdot kg^{-1}$),[50] TiC/$Ni_{12}P_5$//TiC/$Ni_{12}P_5$ (42.6 $Wh \cdot kg^{-1}$ at 1550 $W \cdot kg^{-1}$), [51] TiC/Fe_2O_3//TiC/MnO_2 (23.9 $Wh \cdot kg^{-1}$ at 5400 $W \cdot kg^{-1}$).[52] The assembled pouch cell successfully powered an electric stopwatch (Figures 7h–i and Figure S9a,) for ~1800 s and a mini-fan (Figure S9b) for ~50 s, demonstrating its practical application as a power source.

The remarkable electrochemical performance of the TiC/C//TiN/C asymmetric SC could be attributed to the synergistic effect of the compositions, morphology, and microstructure of the nanocomposite electrodes. The unique 3D hierarchical nanostructures consisting of carbon

nanosheets and active nanoparticles could serve as an electrolyte reservoir and reduce the ion diffusion distance. The carbon nanosheets acted as an ideal support for the high dispersion of active materials (i.e., TiN, TiC) and enabled fast electron transfer. They also minimized the detachment of the active materials during cycling. The nanoparticles of TiN, TiC offered more contact area and exposed active sites with electrolyte, thereby enhancing their electrochemical performance. The presence of oxygen-related bonds and defects facilitated the wettability of electrode materials and provided additional pseudocapacitive contribution. The TiN-TiC cathode-anode couple derived from the same precursor enlarged the potential window, thus improving the electrochemical performance.

To better understand the energy storage mechanism of the asymmetric TiC/C//TiN/C SC and promote the development of high-performance asymmetric SCs and hybrid SCs, it is important to have an in-depth investigation of the charge stored at each side. The electrochemical results of the half cell and full cell studies showed that the energy storage mechanisms for cathode and anode during charge/discharge processes were different because they involved two types of ions. This has significant effects on device performance, such as the working potential window and the specific capacitance. When the SC was in the charge state, the TiN/C cathode would correspond to the adsorption of SO_4^{2-} at the electrode/electrolyte interface, whereby oxygen atoms in SO_4^{2-} would interact with titanium atoms in the TiN/C composite through covalent bonds.[32, 53, 54] On the other hand, the TiC/C anode would undergo a fast and reversible redox reaction, accompanied by the formation of Na_xTiC on its surface.[32, 55, 56] During the discharge process, the SO_4^{2-} adsorbed at the TiN/C cathode interface would desorb and move back to the electrolyte bulk, and the opposite redox reaction would occur at the TiC/C anode side, accompanied by the reversible desorption of Na^+.

$$(Ti_{\text{III}}N)_{surface} + SO_4^{2-} \xrightarrow{Charge} (Ti_{\text{III}}N)_{surface}/(SO_4^{2-})_{ads}$$

$$Ti_{\text{III}}C + Na^+ + e^- \xrightarrow{Charge} Na - Ti_{\text{II}}C$$

$$(Ti_{\text{III}}C)_{surface} + Na^+ \xrightarrow{Charge} (Ti_{\text{III}}C)_{surface}/(Na^+)_{ads}$$

Ex situ XRD studies were conducted to verify the energy storage mechanism occurring at cathode and anode sides of the cell (Figure 8a). To avoid the effect of irreversible reactions occurring in the first cycle, the XRD patterns (Figures 8b and c) were obtained from the second cycle. We observed no new diffraction peaks, and only slight shifts in diffraction peaks (e.g., (200) peak) toward a higher angle for the TiN/C cathode when the voltage was charged from 0.3 to 1.8 V. This could be due to the deviation of electron cloud between titanium atoms in the TiN/C nanocomposite and oxygen atoms in SO_4^{2-} as well as steric effect, [53, 54] causing less electrostatic repulsion of the neighboring layers. [57, 58] In contrast, the diffraction peaks shifted gradually to a lower angle during the discharge process. This indicated that the adsorption/desorption of SO_4^{2-} was a reversible structural evolution process. The contraction/expansion in the interplanar spacing was also observed by HR-TEM images under the different potential states (Figures 8d–f).

For the TiC/C anode, a similar trend of diffraction peaks shifting to a higher angle was observed in the charge process. The contraction of the interplanar distance was attributed to an increase electrostatic attraction between guest Na^+ ions and the TiC lattice.[57, 59, 60] During the discharge process, the (200) peak shifted to a lower angle due to the extraction of Na^+. The change in lattice space was also observed by HR-TEM (Figures 8g–i). These studies demonstrated that the highly reversible redox reactions occurring at the TiC/C anode side mainly contributed to the charge storage without causing obvious phase change. Therefore, it was reasonable to conclude that the charge storage mechanism of the TiC/C//TiN/C device was achieved by combining the reversible

redox reaction accompanying the adsorption/desorption at the TiC/C anode side, and the fast adsorption/desorption process at the TiN/C cathode side. Both the cations and anions played important roles in contributing to the capacitance of the asymmetric SC.

3. Conclusions

A C_3N_4-mediated "one-for-two" strategy has been employed to design and synthesize TiN/C and TiC/C with unique 3D hierarchical nanostructures using $Ti(C_4H_9O)_4$ as the common precursor. The TiN/C nanocomposite cathode and TiC/C nanocomposite anode both exhibited excellent capacitor behavior in 0.5 M Na_2SO_4 electrolyte. The asymmetric TiC/C//TiN/C SC demonstrated outstanding performance, including large specific capacitance (103 $F \cdot g^{-1}$ at 0.5 $A \cdot g^{-1}$), high energy density (45.2 $Wh \cdot kg^{-1}$ at a power density of 535.3 $W \cdot kg^{-1}$), and attractive rate capability (73 $F \cdot g^{-1}$ at 10 $A \cdot g^{-1}$). This asymmetric SC retained 82% of its initial specific capacitance after 4000 cycles, illustrating long-term durability. The remarkable electrochemical performance of the TiC/C//TiN/C SC could be attributed to the synergistic effects between the reversible pseudocapacitive redox reaction occurring at the TiC/C anode side, and the fast adsorption/desorption of anions at the TiN/C cathode side, as well as the unique nanocomposite morphologies and heterostructures, and cathode-anode couple design. The "one-for-two" approach presented herein offers new possibilities for designing advanced electrode materials for energy storage devices.

Authorship Contribution Statement

Wenwen Liu: Conceptualization, Methodology, Investigation, Validation, Writing - original draft, Writing - review & editing. **Jian Liang Cheong:** Conceptualization, Methodology, Writing -

review & editing. **Man-Fai Ng:** Simulation, Visualization, Writing - review & editing. **Jackie Y. Ying:** Conceptualization, Methodology, Supervision, Writing - review & editing.

Declaration of Competing Interest

There are no conflicts to declare.

Acknowledgements

The authors thank Dr. Jinhua Yang for his helpful discussions and comments. This work was supported by the NanoBio Lab, Institute of Materials Research and Engineering (Science and Engineering Research Council, A*STAR, Singapore), and A*Star Career Development Fund <C210812019>. We also acknowledge the National Supercomputing Centre (NSCC) Singapore and A*STAR Computational Resource Centre (A*CRC) of Singapore for the use of the high-performance computing facilities.

Appendix A. Supporting Information

Material synthesis, material characterization, electrochemical measurements, DFT simulation details, photograph of the synthesized materials, Raman of C_3N_4, CV curves and charge/discharge curves of commercial TiN, EIS of TiN/C composite, CV curves and charge/discharge curves of commercial TiC, EIS of TiC/C composite, TEM images of TiN/C after cycling, TEM images of TiC/C after cycling, and photograph of home-made pouch cell are shown in the supporting information.

References

[1] Y. Zhou, H. Qi, J. Yang, Z. Bo, F. Huang, M. S. Islam, X. Lu, L. Dai, R. Amal, C. H. Wang, Z. Han, Two-birds-one-stone: multifunctional supercapacitors beyond traditional energy storage, *Energy Environ. Sci*. 14 (2021) 1854-1896.

[2] Y. Li, J. Xu, T. Feng, Q. Yao, J. Xie, H. Xia, Fe_2O_3 nanoneedles on ultrafine nickel nanotube arrays as efficient anode for high-performance asymmetric supercapacitors, *Adv. Funct. Mater*. 27 (2017) 1606728.

[3] J. Xu, N. Yang, S. Heuser, S. Yu, A. Schulte, H. Schönherr, X. Jiang, Achieving ultrahigh energy densities of supercapacitors with porous titanium carbide/boron-doped diamond composite electrodes, *Adv. Energy Mater*. 9 (2019) 1803623.

[4] Y. Zhang, H. Hua, Z. Wang, B. Luo, W. Xing, L. Li, Z. Yan, L. Wang, Boosting the performance of hybrid supercapacitors through redox electrolyte-mediated capacity balancing, *Nano Energy* 68 (2020) 104226.

[5] T. Zhai, L. Wan, S. Sun, Q. Chen, J. Sun, Q. Xia, H. Xia, Phosphate ion functionalized Co_3O_4 ultrathin nanosheets with greatly improved surface reactivity for high performance pseudocapacitors, *Adv. Mater.* 29 (2017) 1604167.

[6] Y. Jiang, Y. Song, Y. Li, W. Tian, Z. Pan, P. Yang, Y. Li, Q. Gu, L. Hu, Charge transfer in ultrafine LDH nanosheets/graphene interface with superior capacitive energy storage performance, *ACS Appl. Mater. Interfaces* 9 (2017) 37645-37654.

[7] S. Mahadik, S. Surendran, J. Y. Kim, G. Janani, D.-K. Lee, T.-H. Kim, J. K. Kim, U. Sim, Syntheses and electronic structure engineering of transition metal nitrides for supercapacitor applications, *J. Mater. Chem. A* 10 (2022) 14655-14673.

[8] H. Cheng, N. Garcia-Araez, A. L. Hector, S. Soulé, Synthesis of hard carbon-TiN/TiC composites by reacting cellulose with $TiCl_4$ followed by carbothermal nitridation/reduction,

Inorg. Chem. 58 (2019) 5776-5786.

[9] A. Achour, J. B. Ducros, R. L. Porto, M. Boujtita, E. Gautron, L. Le Brizoual, M. A. Djouadi, T. Brousse, Hierarchical nanocomposite electrodes based on titanium nitride and carbon nanotubes for micro-supercapacitors, *Nano Energy* 7 (2014) 104-113.

[10] J. L. Cheong, C. Hu, W. Liu, M.-F. Ng, M. B. Sullvan, J. Y. Ying, 3D carbonaceous nanostructured transition metal nitride, carbonitride and carbide as polysulfide regulators for lithium-sulfur batteries, *Nano Energy* 102 (2022) 107659.

[11] X. Hou, Q. Li, L. Zhang, T. Yang, J. Chen, L. Su, Tunable preparation of chrysanthemum-like titanium nitride as flexible electrode materials for ultrafast-charging/discharging and excellent stable supercapacitors, *J. Power Sources* 396 (2018) 319-326.

[12] S. Dong, X. Chen, L. Gu, X. Zhou, L. Li, Z. Liu, P. Han, H. Xu, J. Yao, H. Wang, X. Zhang, C. Shang, G. Cui, L. Chen, One dimensional MnO_2/titanium nitride nanotube coaxial arrays for high performance electrochemical capacitive energy storage, *Energy Environ. Sci.* 4 (2011) 3502-3508.

[13] S. Hussain, X. Yang, M. K. Aslam, A. Shaheen, M. S. Javed, N. Aslam, B. Aslam, G. Liu, G. Qiao, Robust TiN nanoparticles polysulfide anchor for Li–S storage and diffusion pathways using first principle calculations, *Chem. Eng. J.* 391 (2020) 123595.

[14] W. Li, C. Han, Q. Gu, S. Chou, H. K. Liu, S. X. Dou, Three-dimensional electronic network assisted by TiN conductive pillars and chemical adsorption to boost the electrochemical performance of red phosphorus, *ACS Nano* 14 (2020) 4609-4617.

[15] B. Yao, M. Li, J. Zhang, L. Zhang, Y. Song, W. Xiao, A. Cruz, Y. Tong, Y. Li, TiN paper for ultrafast-charging supercapacitors, *Nano-Micro Letters* 12 (2020) 3.

[16] H. Wang, J. Li, K. Li, Y. Lin, J. Chen, L. Gao, V. Nicolosi, X. Xiao, J.-M. Lee, Transition metal nitrides for electrochemical energy applications, *Chem. Soc. Rev.* 50 (2021) 1354-1390.

[17] P. Qin, C. Huang, B. Gao, C. Pi, J. Fu, X. Zhang, K. Huo, P. K. Chu, Ultrathin carbon layer-encapsulated TiN nanotubes array with enhanced capacitance and electrochemical stability for supercapacitors, *App. Surf. Sci.* 503 (2020) 144293.

[18] X. Xia, Y. Zhang, D. Chao, Q. Xiong, Z. Fan, X. Tong, J. Tu, H. Zhang, H. J. Fan, Tubular TiC fibre nanostructures as supercapacitor electrode materials with stable cycling life and wide-temperature performance, *Energy Environ. Sci.* 8 (2015) 1559-1568.

[19] C. Zhu, P. Yang, D. Chao, X. Wang, X. Zhang, S. Chen, B. K. Tay, H. Huang, H. Zhang, W. Mai, H. J. Fan, All metal nitrides solid-state asymmetric supercapacitors, *Adv. Mater.* 27 (2015) 4566-4571.

[20] N. Sun, D. Zhou, W. Liu, S. Shi, Z. Tian, F. Liu, S. Li, J. Wang, F. Ali, Tailoring surface chemistry and morphology of titanium nitride electrode for on-chip supercapacitors, *ACS Sustainable Chem. Eng.* 8 (2020) 7869-7878.

[21] C. Yang, M. Sun, H. Lu, Asymmetric all-metal-oxide supercapacitor with superb cycle performance, *Chem. Eur. J.* 24 (2018) 6169-6177.

[22] C. Guan, W. Zhao, Y. Hu, Z. Lai, X. Li, S. Sun, H. Zhang, A. K. Cheetham, J. Wang, Cobalt oxide and N-doped carbon nanosheets derived from a single two-dimensional metal–organic framework precursor and their application in flexible asymmetric supercapacitors, *Nanoscale Horiz.* 2 (2017) 99-105.

[23] D. Wang, M. Al-Mamun, W. Gong, Y. Lv, C. Chen, Y. Lin, G. Wang, H. Zhang, H. Zhao, Converting Co^{2+}-impregnated g-C_3N_4 into N-doped CNTs-confined Co nanoparticles for

efficient hydrogenation rearrangement reactions of furanic aldehydes, *Nano Res.* 14 (2021) 2846-2852.

[24] J. H. Han, J. H. Bang, A hollow titanium oxynitride nanorod array as an electrode substrate prepared by the hot ammonia-induced Kirkendall effect, *J. Mater. Chem. A* 2 (2014) 10568-10576.

[25] C. Gong, C. Yan, J. Zhang, X. Cheng, H. Pan, C. Zhang, L. Yu, Z. Zhang, Room-temperature ferromagnetism evolution in nanostructured titanium nitride superconductors – The influence of structural defects, *J. Mater. Chem.* 21 (2011) 15273-15278.

[26] D. T. Dam, K.-D. Nam, H. Song, X. Wang, J.-M. Lee, Partially oxidized titanium carbonitride as a non-noble catalyst for oxygen reduction reactions, *Int. J. Hydrog. Energy* 37 (2012) 15135-15139.

[27] Y. Han, X. Yue, Y. Jin, X. Huang, P. K. Shen, Hydrogen evolution reaction in acidic media on single-crystalline titanium nitride nanowires as an efficient non-noble metal electrocatalyst, *J. Mater. Chem. A* 4 (2016) 3673-3677.

[28] P. Yang, D. Chao, C. Zhu, X. Xia, Y. Zhang, X. Wang, S. Peng, B. K. Tay, Z. Shen, W. Mai, H. J. Fan, Ultrafast-charging supercapacitors based on corn-like titanium nitride nanostructures, *Adv. Sci*. 3 (2016) 1500299.

[29] P. Sun, R. Lin, Z. Wang, M. Qiu, Z. Chai, B. Zhang, H. Meng, S. Tan, C. Zhao, W. Mai, Rational design of carbon shell endows TiN@C nanotube based fiber supercapacitors with significantly enhanced mechanical stability and electrochemical performance, *Nano Energy* 31 (2017) 432-440.

[30] Y. Zhang, L. Yu, R. Hu, J. Zhang, Y. Wang, R. Niu, X. Qian, J. Zhu, Biomass-derived C/N co-doped $Ni(OH)_2/Ni_xS_y$ with a sandwich structure for supercapacitors, *J. Mater. Chem. A*

6 (2018) 17417-17425.

[31] W. Guo, C. Yu, S. Li, J. Yang, Z. Liu, C. Zhao, H. Huang, M. Zhang, X. Han, Y. Niu, J. Qiu, High-stacking-density, superior-roughness LDH bridged with vertically aligned graphene for high-performance asymmetric supercapacitors, *Small* 13 (2017) 1701288.

[32] V. Shrivastav, S. Sundriyal, P. Goel, V. Shrivastav, U. K. Tiwari, A. Deep, ZIF-67 derived Co_3S_4 hollow microspheres and WS_2 nanorods as a hybrid electrode material for flexible 2V solid-state supercapacitor, *Electrochim. Acta* 345 (2020) 136194.

[33] S. Dong, X. Chen, L. Gu, X. Zhou, H. Xu, H. Wang, Z. Liu, P. Han, J. Yao, L. Wang, G. Cui, L. Chen, Facile preparation of mesoporous titanium nitride microspheres for electrochemical energy storage, *ACS Appl. Mater. Interfaces* 3 (2011) 93-98.

[34] Y. Xu, J. Wang, B. Ding, L. Shen, H. Dou, X. Zhang, General strategy to fabricate ternary metal nitride/carbon nanofibers for supercapacitors, *ChemElectroChem* 2 (2015) 2020-2026.

[35] S. Dong, X. Chen, L. Gu, X. Zhou, H. Wang, Z. Liu, P. Han, J. Yao, L. Wang, G. Cui, L. Chen, TiN/VN composites with core/shell structure for supercapacitors, *Mater. Res. Bull.* 46 (2011) 835-839.

[36] X. Zhou, C. Shang, L. Gu, S. Dong, X. Chen, P. Han, L. Li, J. Yao, Z. Liu, H. Xu, Y. Zhu, G. Cui, Mesoporous coaxial titanium nitride-vanadium nitride fibers of core–shell structures for high-performance supercapacitors, *ACS Appl. Mater. Interfaces* 3 (2011) 3058-3063.

[37] C. Chen, X. Yang, MnO_2 modified TiN nanotube arrays on Ti mesh for flexible supercapacitors electrode, *RSC Adv.* 7 (2017) 56440-56446.

[38] K. Jayaramulu, D. P. Dubal, B. Nagar, V. Ranc, O. Tomanec, M. Petr, K. K. R. Datta, R. Zboril, P. Gómez-Romero, R. A. Fischer, Ultrathin hierarchical porous carbon nanosheets

for high-performance supercapacitors and redox electrolyte energy storage, *Adv. Mater.* 30 (2018) 1705789.

[39] J. G. Wang, H. Liu, X. Zhang, M. Shao, B. Wei, Elaborate construction of N/S-co-doped carbon nanobowls for ultrahigh-power supercapacitors, *J. Mater. Chem. A* 6 (2018) 17653-17661.

[40] T. Chen, M. Li, S. Song, P. Kim, J. Bae, Biotemplate preparation of multilayered TiC nanoflakes for high performance symmetric supercapacitor, *Nano Energy* 71 (2020) 104549.

[41] M. U. Rani, K. Nanaji, T. N. Rao, A. S. Deshpande, Corn husk derived activated carbon with enhanced electrochemical performance for high-voltage supercapacitors, *J. Power Sources* 471 (2020) 228387.

[42] C. Li, X. Zhang, Z. Lv, K. Wang, X. Sun, X. Chen, Y. Ma, Scalable combustion synthesis of graphene-welded activated carbon for high-performance supercapacitors, *Chem. Eng. J.* 414 (2021) 128781.

[43] A. Ignaszak, C. Song, W. Zhu, J. Zhang, A. Bauer, R. Baker, V. Neburchilov, S. Ye, S. Campbell, Titanium carbide and its core-shelled derivative TiC@TiO_2 as catalyst supports for proton exchange membrane fuel cells, *Electrochim. Acta* 69 (2012) 397-405.

[44] H. B. Parse, I. Patil, S. Ingavale, C. Manohar, V. A. L. Roy, B. Kakade, Efficient oxygen electroreduction kinetics by titanium carbide@nitrogen doped carbon nanocomposite, *Int. J. Hydrog. Energy* 44 (2019) 23649-23657.

[45] G. Pan, F. Cao, Y. Zhang, Synthesis of titanium carbide/carbon composites for supercapacitor application, *Mater. Res. Bull.* 137 (2021) 111172.

[46] Y. Ren, J. Dai, B. Pang, X. Liu, J. Yu, Synergistic enhancement of electrochemical performance of electrospun TiC/C hybrid nanofibers for supercapacitor application,

Electrochim. Acta 176 (2015) 402-409.

[47] Y. Zhong, X. Xia, J. Zhan, Y. Wang, X. Wang, J. Tu, Monolayer titanium carbide hollow sphere arrays formed via an atomic layer deposition assisted method and their excellent high-temperature supercapacitor performance, *J. Mater. Chem. A* 4 (2016) 18717-18722.

[48] H. Y. Wang, B. Li, J. X. Teng, H. L. Zhu, Y. X. Qi, L. W. Yin, H. Li, N. Lun, Y.-J. Bai, N-doped carbon-coated TiN exhibiting excellent electrochemical performance for supercapacitors, *Electrochim. Acta* 257 (2017) 56-63.

[49] T. Zheng, M. H. Tahmasebi, B. Li, Y. Li, S. Ran, T. S. Glen, K.-H. Lam, I.-S. Choi, S. T. Boles, Sputtered titanium nitride films on titanium foam substrates as electrodes for high-power electrochemical capacitors, *ChemElectroChem* 5 (2018) 2199-2207.

[50] M. Li, K. Zhu, Z. Meng, R. Hu, J. Wang, C. Wang, P. K. Chu, Efficient coupling of MnO_2/TiN on carbon cloth positive electrode and Fe_2O_3/TiN on carbon cloth negative electrode for flexible ultra-fast hybrid supercapacitors, *RSC Adv.* 11 (2021) 35726-35736.

[51] J. Xu, N. Yang, S. Yu, A. Schulte, H. Schönherr, X. Jiang, Ultra-high energy density supercapacitors using a nickel phosphide/nickel/titanium carbide nanocomposite capacitor electrode, *Nanoscale* 12 (2020) 13618-13625.

[52] R. Feng, M. Li, Y. Wang, J. Lin, K. Zhu, J. Wang, C. Wang, P. K. Chu, High-performance multi-dimensional nitrogen-doped N+MnO_2@TiC/C electrodes for supercapacitors, *Electrochim. Acta* 370 (2021) 137716.

[53] Z. Huang, T. Wang, H. Song, X. Li, G. Liang, D. Wang, Q. Yang, Z. Chen, L. Ma, Z. Liu, B. Gao, J. Fan, C. Zhi, Effects of anion carriers on capacitance and self-discharge behaviors of zinc ion capacitors, *Angew. Chem. Int. Ed.* 60 (2021) 1011-1021.

[54] I. Aldama, V. Barranco, M. Kunowsky, J. Ibañez, J. M. Rojo, Contribution of cations and anions of aqueous electrolytes to the charge stored at the electric electrolyte/electrode interface of carbon-based supercapacitors, *J. Phys. Chem. C* 121 (2017) 12053-12062.

[55] Y. Zhong, X. Xia, F. Shi, J. Zhan, J. Tu, H. J. Fan, Transition metal carbides and nitrides in energy storage and conversion, *Adv. Sci.* 3 (2016) 1500286.

[56] E. Kao, C. Yang, R. Warren, A. Kozinda, L. Lin, ALD titanium nitride on vertically aligned carbon nanotube forests for electrochemical supercapacitors, *Sens. Actuators A* 240 (2016) 160-166.

[57] T. Jin, P.-F. Wang, Q.-C. Wang, K. Zhu, T. Deng, J. Zhang, W. Zhang, X.-Q. Yang, L. Jiao, C. Wang, Realizing complete solid-solution reaction in high sodium content P2-type cathode for high-performance sodium-ion batteries, *Angew. Chem. Int. Ed.* 59 (2020) 14511-14516.

[58] J. Wang, Y. Wang, D. H. Seo, T. Shi, S. Chen, Y. Tian, H. Kim, G. Ceder, A high-energy NASICON-type cathode material for Na-ion batteries, *Adv. Energy Mater.* 10 (2020) 1903968.

[59] X. Mu, D. Wang, F. Du, G. Chen, C. Wang, Y. Wei, Y. Gogotsi, Y. Gao, Y. Dall'Agnese, Revealing the pseudo-intercalation charge storage mechanism of MXenes in acidic electrolyte, *Adv. Funct. Mater.* 29 (2019) 1902953.

[60] Z. Tian, X. Tong, G. Sheng, Y. Shao, L. Yu, V. Tung, J. Sun, R. B. Kaner, Z. Liu, Printable magnesium ion quasi-solid-state asymmetric supercapacitors for flexible solar-charging integrated units, *Nat. Commun.* 10 (2019) 4913.

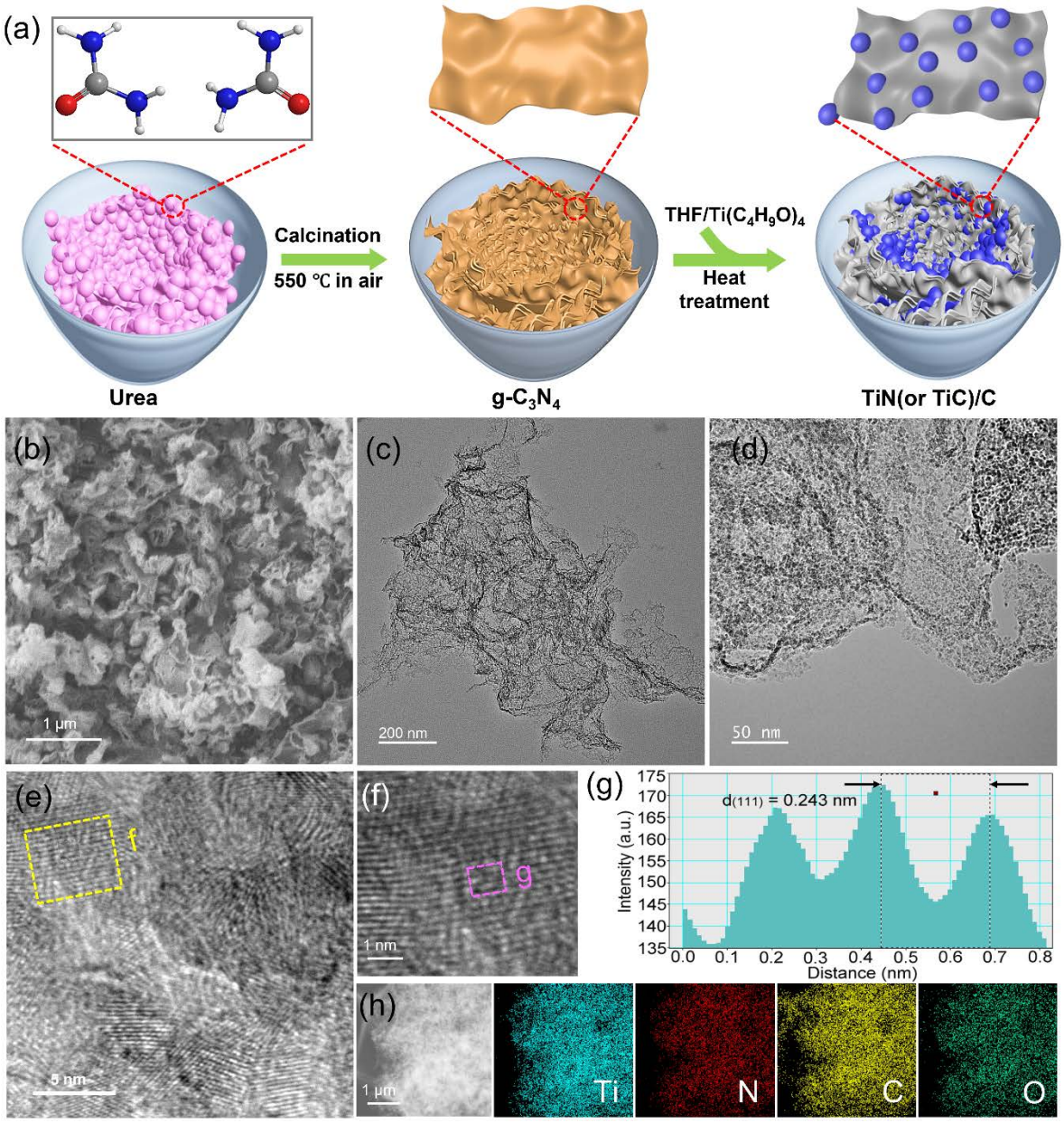

Figure 1. (a) Schematic diagram of the synthesis of TiN/C and TiC/C nanocomposites. (b) SEM image, (c–f) TEM images, and (g) the corresponding profile of interlayer spacing of the boxed image in (f), (h) STEM and EDX elemental mapping of TiN/C nanocomposite.

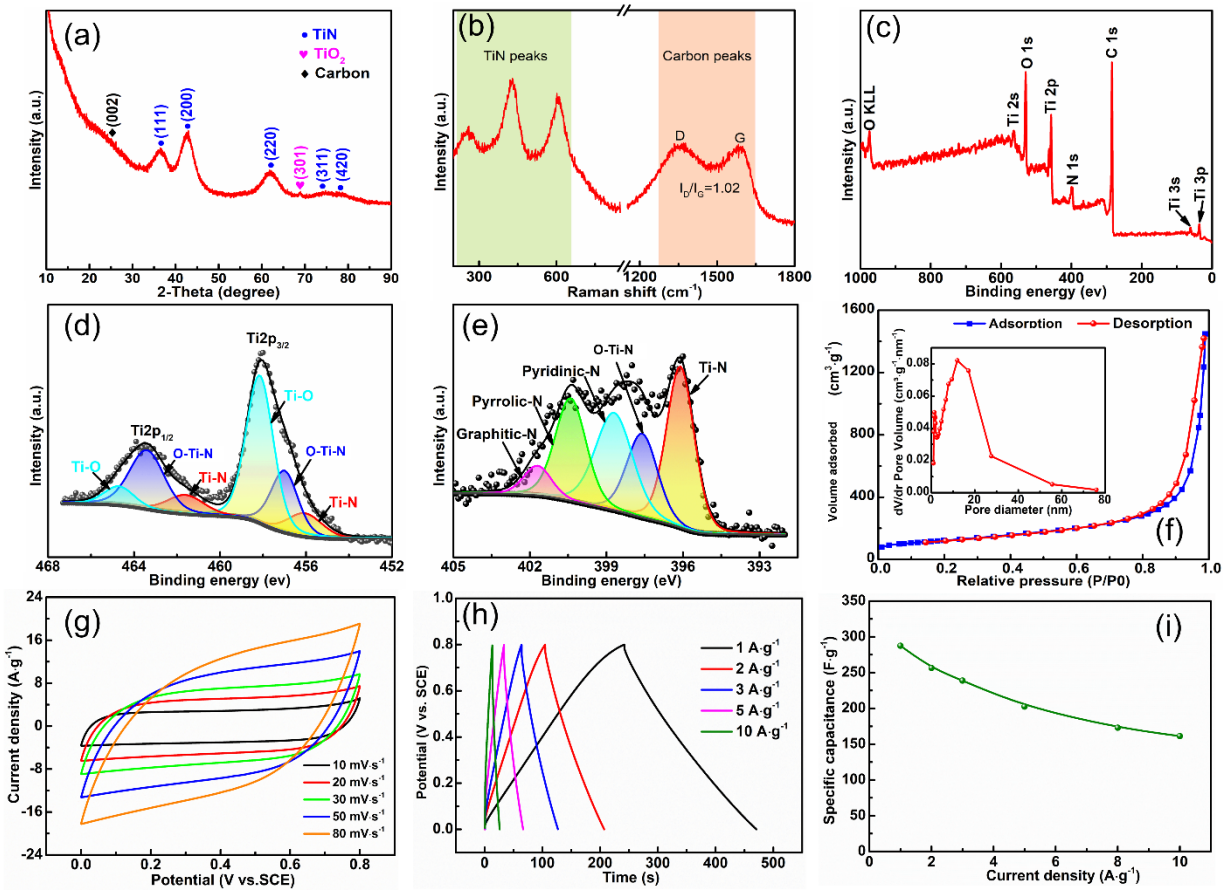

Figure 2. (a) XRD pattern, (b) Raman spectrum, XPS (c) survey, (d) Ti2p and (e) N1s spectra, (f) nitrogen adsorption-desorption isotherms and (inset) desorption pore size distribution, (g) CV curves, (h) GCD curves, and (i) variation of specific capacitance with current densities for TiN/C nanocomposite.

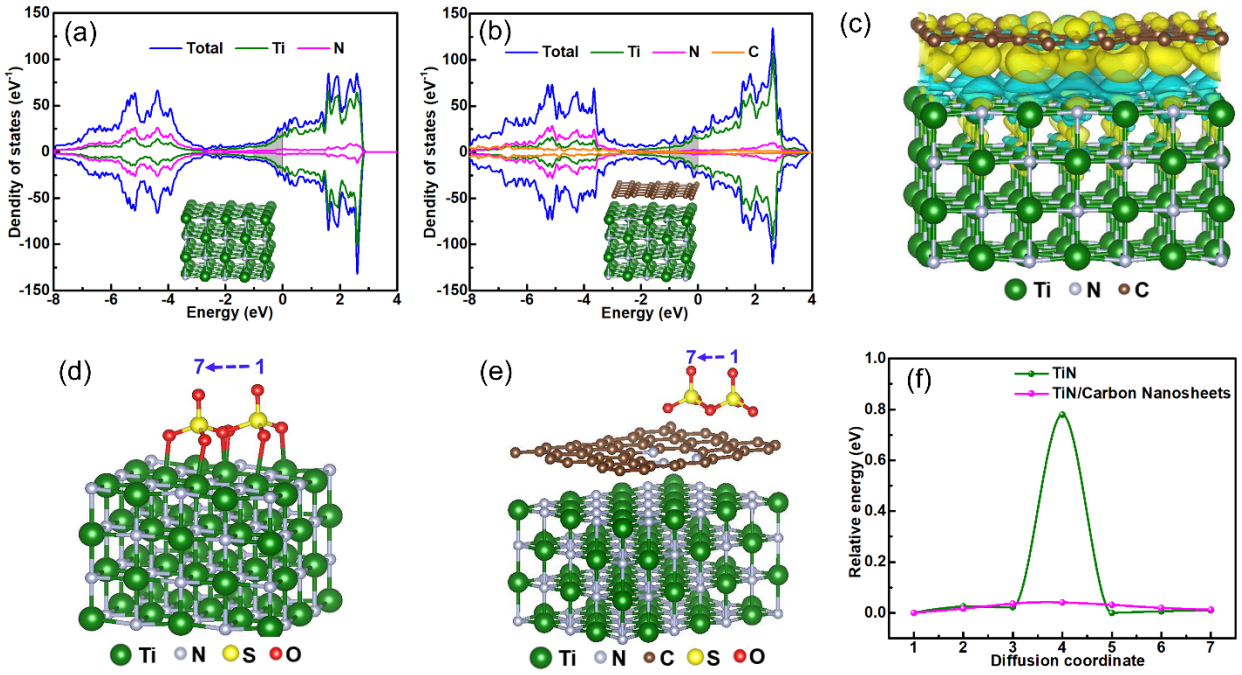

Figure 3. Density of states and partial density of states of the models of (a) pure TiN and (b) TiN/C nanocomposite. Insets of (a) and (b) are the corresponding structure of TiN and TiN/C, respectively. The Fermi level is set at 0 eV. (c) Charge density difference plot of the TiN/C nanocomposite. The yellow and cyan isosurfaces represent charge accumulation and depletion, respectively. Lowest energy diffusion path of SO_4^{2-} on (d) pure TiN surface and (e) TiN/C surface. (f) Diffusion barriers of SO_4^{2-} on pure TiN surface and TiN/C surface.

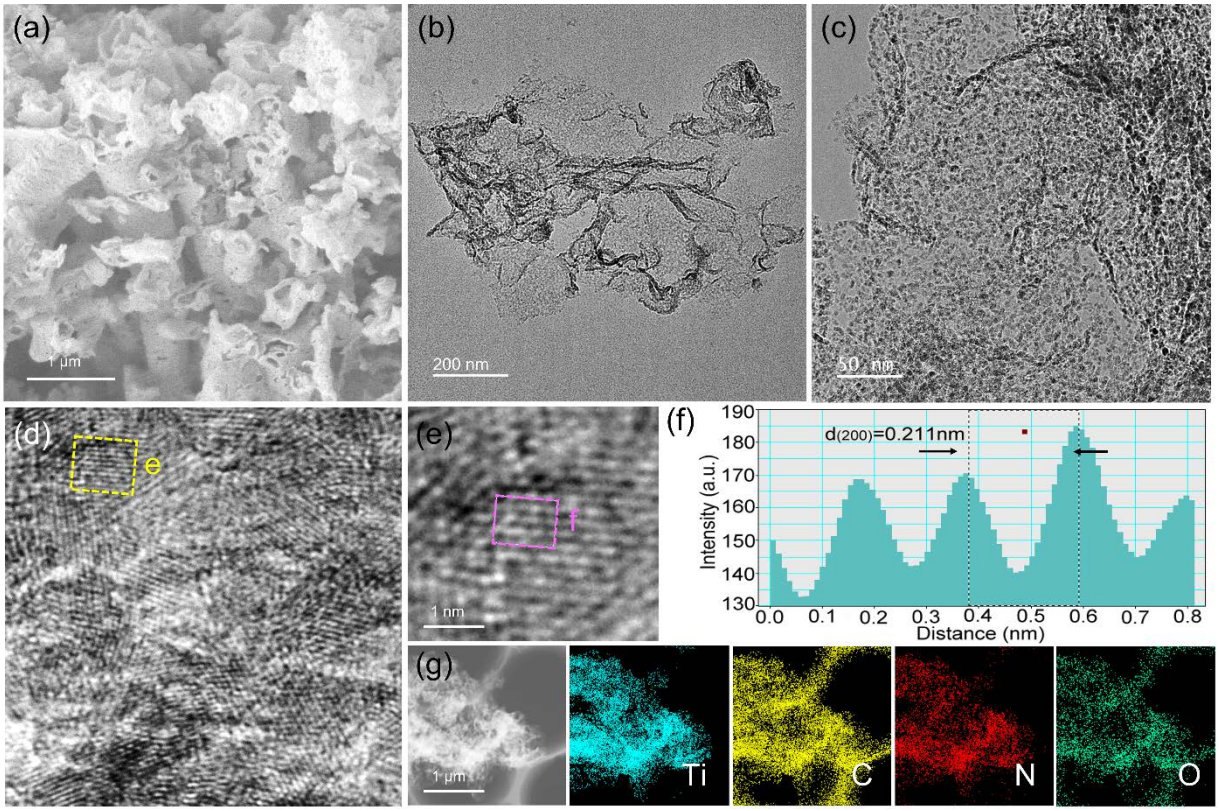

Figure 4. (a) SEM image, (b–e) TEM images and (f) the corresponding profile of interlayer spacing of the boxed image in (e), (g) TEM and EDX elemental mapping of TiC/C nanocomposite.

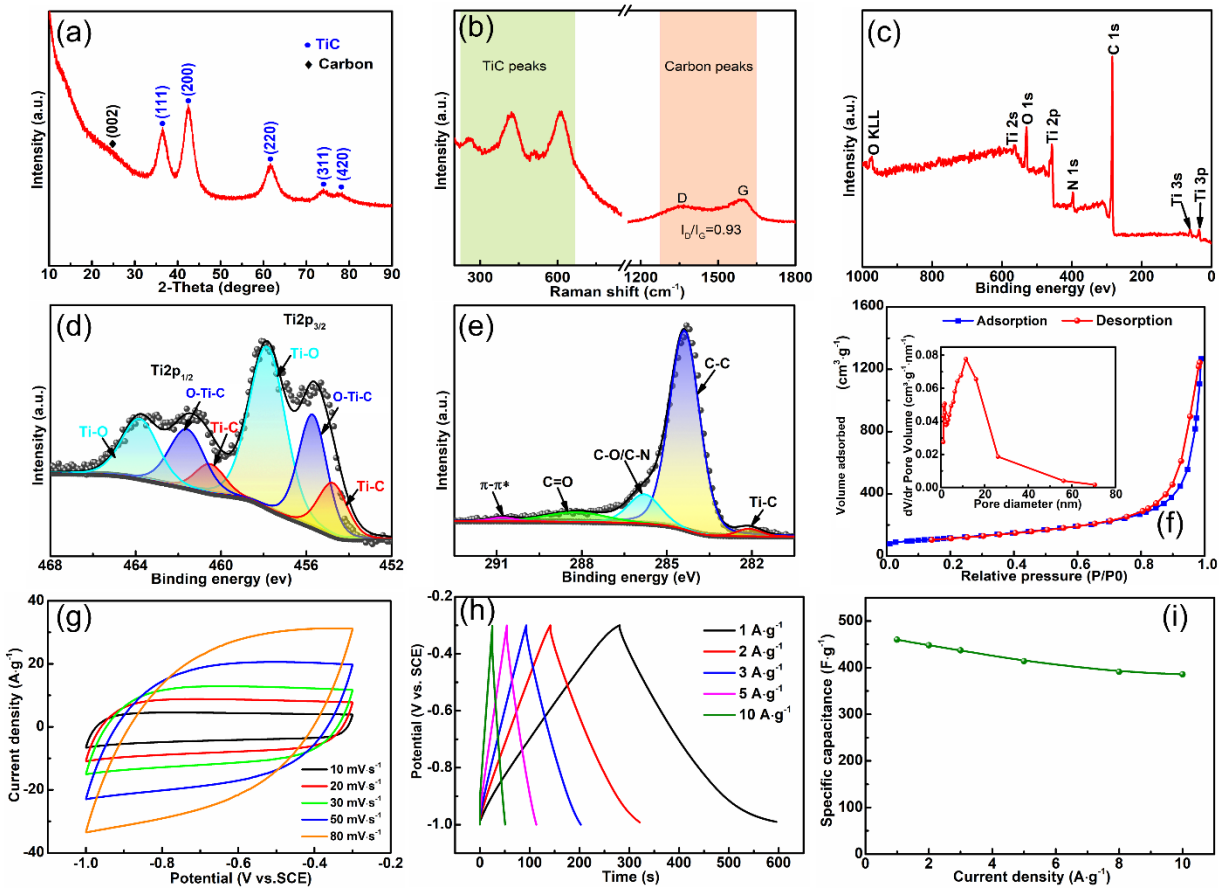

Figure 5. (a) XRD pattern, (b) Raman spectrum, XPS (c) survey, (d) Ti2p and (e) C1s spectra, (f) nitrogen adsorption-desorption isotherms and (inset) desorption pore size distribution, (g) CV curves, (h) GCD curves, and (i) variation of specific capacitance with current densities for TiC/C nanocomposite.

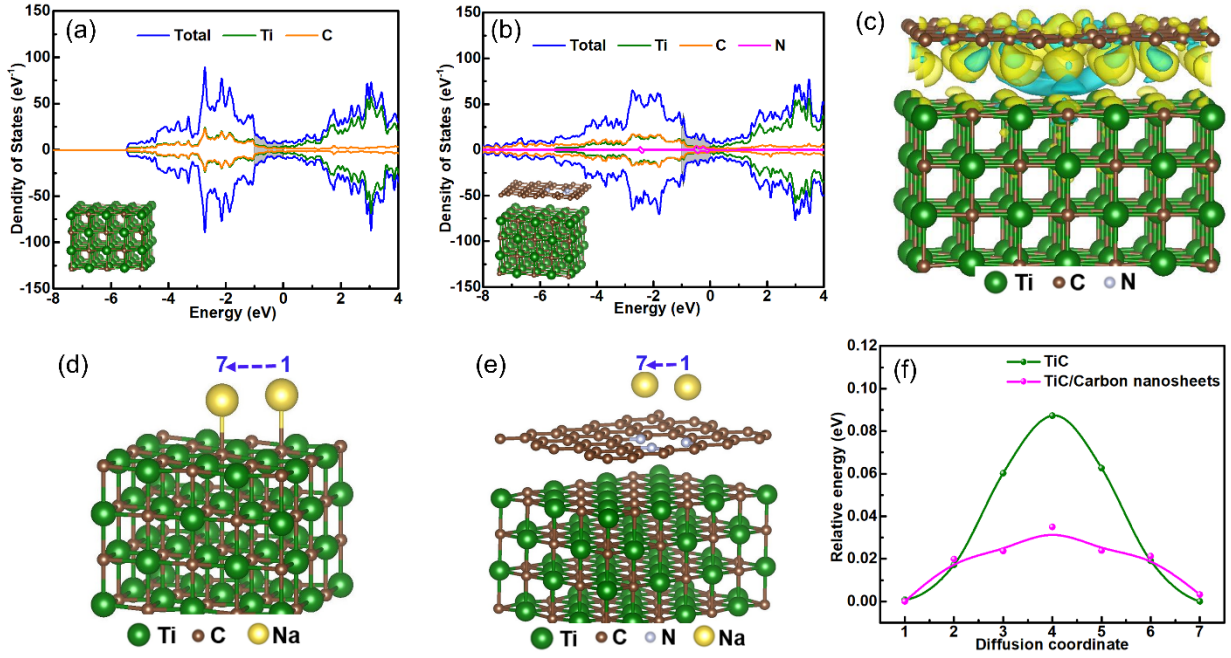

Figure 6. Density of states and partial density of states of the models of (a) pure TiC and (b) TiC/C nanocomposite. Insets of (a) and (b) are the corresponding structure of TiC and TiC/C, respectively. The Fermi level is set at 0 eV. (c) Charge density difference plot of the TiC/C nanocomposite. The yellow and cyan isosurfaces represent charge accumulation and depletion, respectively. Lowest energy diffusion path of Na^+ on (d) pure TiC surface and (e) TiC/C surface. (f) Diffusion barriers of Na^+ on pure TiC surface and TiC/C surface.

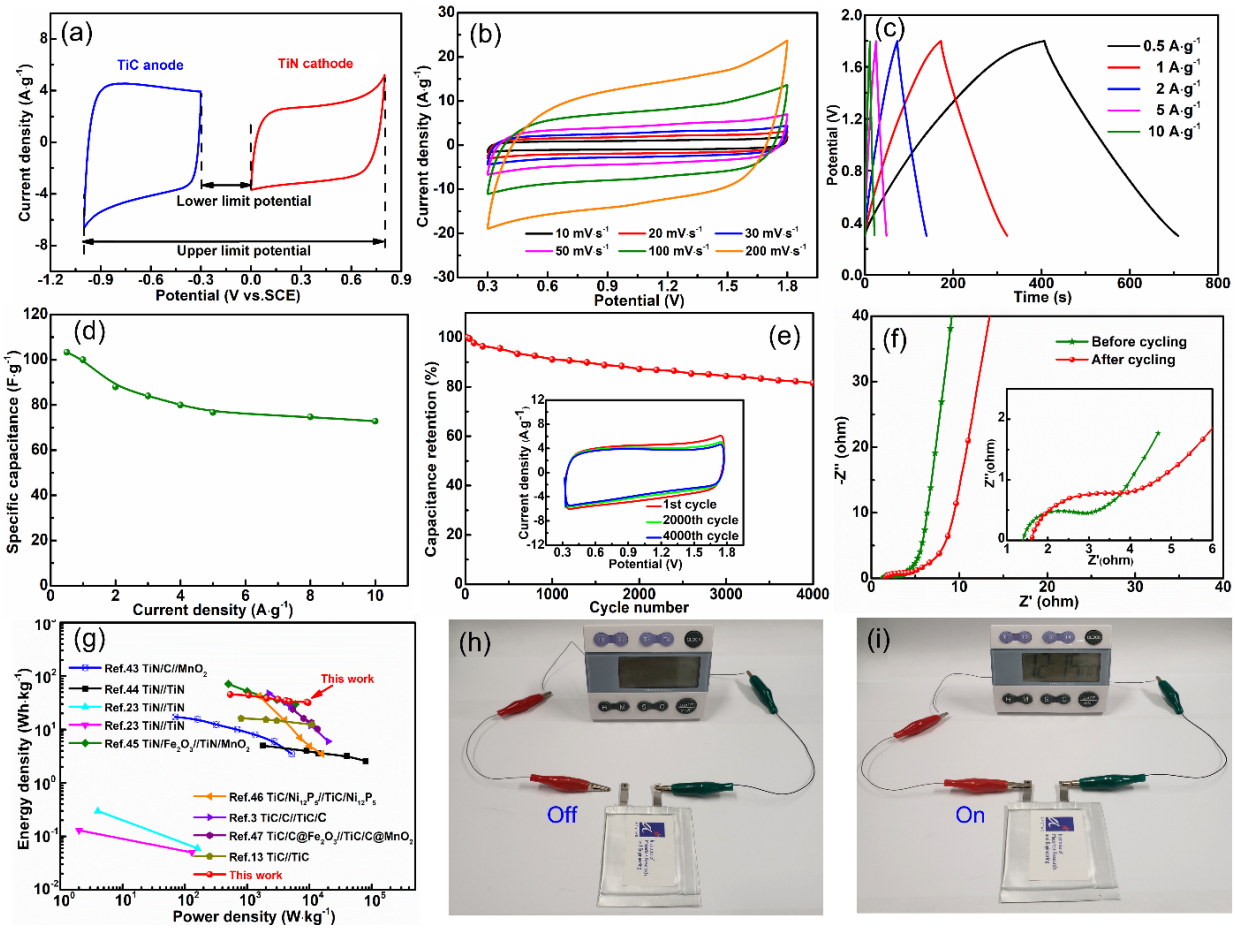

Figure 7. (a) CV curves of TiN/C and TiC/C nanocomposite electrodes at 10 $mV \cdot s^{-1}$. (b) CV curves, (c) GCD curves, (d) rate capability, (e) cycling stability, (f) EIS before and after cycling, (g) Ragone plot of TiC/C//TiN/C asymmetric SCs. Photographs of pouch cell type TiC/C//TiN/C asymmetric SCs powering a stopwatch in the (h) off and (i) on states.

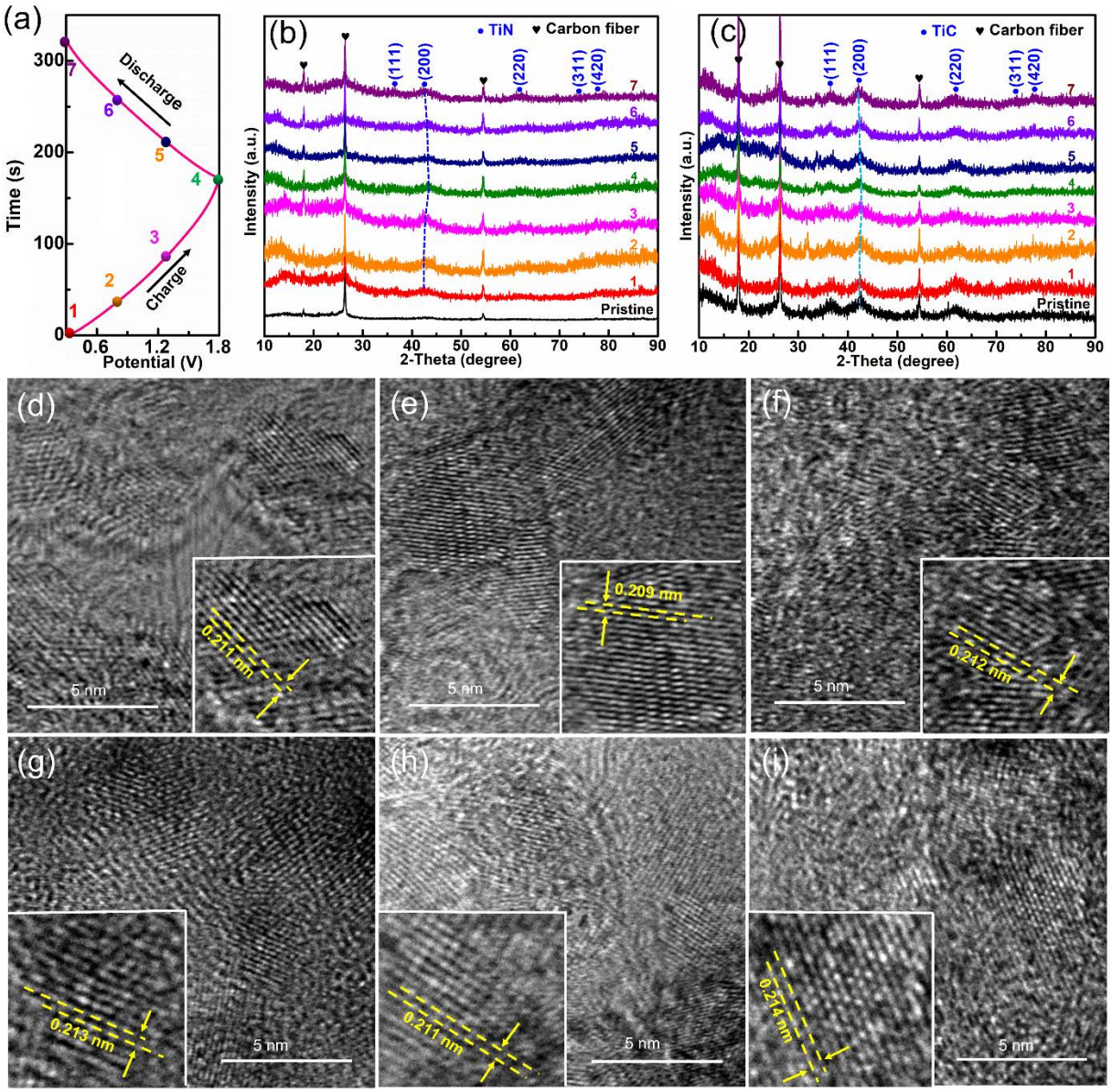

Figure 8. (a) Charge/discharge curve of TiC/C//TiN/C asymmetric SC at 1 A·g^{-1}. *Ex situ* XRD patterns of (b) the TiN/C electrode and (c) the TiC/C electrode at different voltages marked in (a). TEM images of the TiN/C electrode at (d) 0.3 V and (e) 1.8 V under the charge process, and (f) 0.3 V under the discharge process. TEM images of the TiC/C electrode at (g) 0.3 V and (h) 1.8 V under the charge process, and (i) 0.3 V under the discharge process.